Changes in 1958-2019 Greenland Surface Mass Balance are Attributable to both Greenhouse Gases and Anthropogenic Aerosols

Yan-Ning Kuo[1], Riley Culberg[1], and Flavio Lehner[1,2]

[1]Department of Earth and Atmospheric Sciences, Cornell University, Ithaca, NY, USA
[2]Polar Bears International, Bozeman, MT, USA

Correspondence: Yan-Ning Kuo (yk545@cornell.edu)

Abstract. Greenland Ice Sheet (GrIS) mass loss is a main contributor to rising Global Mean Sea Level (GMSL), exhibiting decadal variability due to surface mass balance (SMB) changes. Greenhouse gases (GHG) have long been identified as a key driver of GrIS mass loss through warming-induced runoff. However, there has not been a formal attribution of historical GrIS SMB changes to GHG and the potential role for other forcings such as anthropogenic aerosols (AAER). Here, we use the Community Earth System Model version 2 large ensemble and single forcing large ensemble (CESM2-LE and CESM2-SFLE) to formulate a detection and attribution analysis for historical GrIS SMB changes. We show that the decadal variability of SMB is forced by historical radiative forcing attributable to both GHG and AAER through their forced changes of runoff. This highlights that, in addition to the frequently mentioned GHG, AAER also contributes to SMB changes during the historical period. GHG influences GrIS runoff mainly through long-term radiatively-forced warming, while AAER influences it through the decadal variability of atmospheric circulation that projects onto a Greenland blocking pattern, leading to relative cooling from cyclonic circulation over Greenland pre-1980 and relative warming from anti-cyclonic circulation thereafter. The attribution of SMB, and specifically runoff, to AAER has a lower signal-to-noise ratio (S/N) than the attribution to GHG due to both a weaker signal and wider confidence intervals. The lower S/N in attributing runoff changes to AAER is partly due to a smaller temperature response in AAER than in GHG and partly due to a mean state temperature dependency of the runoff sensitivity. In simulations with only AAER, the climate is colder than in simulations with all forcings or only GHG, leading to more time below freezing when temperature variations do not affect runoff as much. We resolve this issue by comparing simulations with all forcings with simulations in which everything-but-AAER is changing, thereby stressing the need to account for mean state dependencies when conducting detection and attribution with single forcing simulations.

1 Introduction

The global mean sea level (GMSL) has been rising at an averaged rate of 1.56 mm/year since 1900 (Frederikse et al., 2020; Hay et al., 2015; Church et al., 2011) and has accelerated to 3.3 mm/year since the 1990s (Chen et al., 2017; Church et al., 2011). A growing contribution to GMSL rise is from the ocean mass increase (barystatic sea level rise), due to freshwater input to the ocean from terrestrial water, mountain glaciers, and polar ice sheets, including both the Greenland Ice Sheet (GrIS) and Antarctic Ice Sheet. Glaciers remain the least constrained component of the climate change-driven sea level rise (IPCC AR6, 2023). Among these glacial GMSL sources, the GrIS is one of the largest barystatic sea level contributors to GMSL since 1900 (accounting for 29% of the total GMSL increase; Frederikse et al. 2020). Along with contributing to GMSL rise, GrIS mass loss can further increase regional sea level rise rate, such as for the North American East Coast (Mitrovica et al., 2001), resulting in higher risk of coastal flooding (Wdowinski et al., 2016).

GrIS mass loss comes from two factors (Mouginot et al., 2019): (1) changes in the surface mass balance (SMB), defined as the difference between precipitation, evaporation/sublimation, and runoff, and (2) changes in ice discharge related to glacial dynamics, manifested in calving and ocean melting trends. Observational records show that declining GrIS SMB has become an increasingly important contributor to rising GMSL in recent decades (Enderlin et al., 2014; Kjeldsen et al., 2015; Mouginot et al., 2019) and GrIS SMB change is identified as the largest source of GMSL uncertainty in future projections (Pattyn et al., 2018). Thus, understanding why the SMB has changed historically can be informative for projecting future changes of GMSL due to GrIS mass loss.

GrIS SMB reduction has been linked to rising air temperature over Greenland, as warming leads to more surface melting and runoff (Trusel et al., 2018; van Kampenhout et al., 2020; Thompson-Munson et al., 2024). Greenhouse Gases (GHG) amplify warming over the Arctic (Wu et al., 2024), and the consequent runoff increase is consistent with the monotonic long-term decline in GrIS SMB projected for the future under strong radiative forcing scenarios (Hofer et al., 2020). However, there has not been a formal attribution of historical GrIS SMB changes to radiative forcing, despite the emerging signal from GHG-induced global mean temperature warming in recent decades (Deser et al., 2020a). The GrIS SMB decline since the 1990s has also been linked to the increasing frequency of subsidence-induced warming from Greenland blocking, itself linked to the negative phase of the North Atlantic Oscillation (NAO). NAO-related GrIS SMB change has thus far been treated as internal variability on decadal time scales (Sherman et al., 2020; Brils et al., 2023; Hanna et al., 2022). However, new literature attributes the negative NAO transition to anthropogenic aerosols (AAER; Dong and Sutton, 2021) and provides evidence of AAER-forced historical decadal variability for different aspects of North Atlantic climate, including storm tracks (Kang et al., 2024) and sea surface temperatures (SSTs; He et al., 2023). We hypothesize that internal variability might not be the only reason for the recent decadal GrIS SMB changes; instead, both GHG and AAER could have also contributed.

Unlike GHG, historical AAER emissions had a non-monotonic spatio-temporal trajectory, owing to, for example, the timing of social-economic development and air quality regulations in different countries (Persad et al., 2022). This heterogeneous characteristic of AAER has been argued to induce historical decadal variability in various aspects of the Earth's climate; prominent recent examples include tropical sea surface temperature (SST) patterns (Hwang et al., 2024; Dittus et al., 2021; Takahashi and Watanabe, 2016), regional hydroclimate change (Kuo et al., 2023), and mid-latitude circulation (Dow et al., 2021; Oudar et al., 2018). Together with the literature supporting AAER-forced historical decadal variability of North Atlantic climate, we hypothesize that AAER contributes to GrIS SMB changes through its impacts on a circulation pattern projected onto NAO.

However, the forced response to AAER often has a low signal-to-noise ratio (S/N; Dittus et al., 2021; Oudar et al., 2018; Kuo et al., 2025), and so do externally forced NAO changes (McKenna and Maycock, 2021; Scaife and Smith, 2018). Different external radiative forcings can also create nonlinear (or non-additive) responses in the climate system (Simpson et al., 2023;

Kuo et al., 2025). As such, nonlinear interactions between AAER and GHG forcings cannot be captured in the single forcing runs of AAER-only or GHG-only simulations. New climate model large ensembles are designed to better isolate subtle signals and responses to individual forcings from internal variability (Deser et al., 2020b). Therefore, in this study, we utilize the Community Earth System Model version 2 (CESM2; Danabasoglu et al., 2020) large ensemble (CESM2-LE; Rodgers et al., 2021) and its single forcing large ensemble (CESM2-SFLE) with both *forcing-only* and *all-but-forcing* experimental setups (Simpson et al., 2023) to better understand whether the historical decadal variability of GrIS SMB is forced by both GHG and AAER.

In this paper, we apply the detection and attribution (D&A) framework from Allen and Stott (2003) to formally assess whether historical radiative forcings can account for GrIS SMB changes between 1958-2019. We demonstrate that both GHG and AAER contributed to the 1958-2019 GrIS SMB changes and highlight a previously underappreciated source of uncertainty in D&A when the climate response has mean state temperature dependency. This mean state temperature dependency can lead to different S/N for the attribution to GHG compared to AAER. Finally, we will discuss implications of these uncertainties for the general D&A framework.

2 Data and Methods

2.1 Data

2.1.1 Reference data

In this study, reconstruction data, reanalysis data, and a regional climate model simulation driven by reanalysis since 1958 are included as reference data for the historical period. Frederikse et al. (2020)'s reconstruction for GrIS mass loss was used to assess the impact of SMB change on GrIS GMSL contributions since 1958. The Frederikse et al. (2020)'s reconstruction data comes from a Monte Carlo simulation perturbing the known prior estimate based on three estimates of GrIS mass loss data, including a reconstruction from geological inference of historical ice sheet surface elevation (Kjeldsen et al., 2015), an input-output estimate (Mouginot et al., 2019), and a synthesis of satellite observations with a multi-method assessment (Bamber et al., 2018). With 5000 ensemble members, this reconstruction provides a range of observational uncertainty of the GMSL contribution from GrIS mass loss. To understand the drivers of the GrIS GMSL contribution, we use 1958-2019 annual mean SMB, precipitation (P), and runoff (R), averaged over the GrIS, from the polar regional climate model RACMO2.3p2 simulation forced with the reanalysis data sets from ECMWF Reanalysis (ERA), hereafter RACMO-ERA (Noël et al., 2022). RACMO-ERA is run at 5.5 km resolution and statistically downscaled to 1km (Noël et al., 2022). This RACMO-ERA simulation has been compared against in-situ meteorological data and point measurements of GrIS SMB and showed good agreement with these observations (Noël et al., 2018). Here, these RACMO-ERA outputs are treated as the reference data to formulate a D&A analysis. Additionally, annual means of near-surface temperature at 2m (TAS) and 500 hPa geopotential height (Z500) from monthly gridded ERA5 reanalysis (Hersbach et al., 2020) are included to investigate the atmospheric drivers of the SMB changes.

2.1.2 CESM2 large ensemble and single forcing large ensemble (CESM2-LE and CESM2-SFLE)

CESM2-LE and CESM2-SFLE are used for the D&A analysis. CESM2 (Danabasoglu et al., 2020) is a climate model developed by the National Center for Atmospheric Research (NCAR). It includes a land ice model (CISM; Lipscomb et al., 2019) of the GrIS at 4 km spatial resolution. CESM2-LE and CESM2-SFLE are run under compsets with a fixed ice sheet topography so that CISM does not feed back to other parts of the climate system but provides the finer grids to downscale SMB. CESM2 has been evaluated against observations and shown to capture the variability of GrIS SMB well (van Kampenhout et al., 2020; Noël et al., 2020; Noël et al., 2022).

We take the 50-member ensemble from CESM2-LE (Rodgers et al., 2021) that is forced with the full historical radiative forcings (ALL), using smoothed biomass burning forcing (*smbb*). Each ensemble member differs from the others due to initial condition perturbations (see Rodgers et al., 2021) to quantify the uncertainty originating from internal variability. CESM2-SFLE (Simpson et al., 2023) uses the same CESM2 version but instead of the ALL forcing, individual forcings are applied in isolation. We use the 15-member GHG and AAER simulations, as GHG and AAER are two dominant anthropogenic forcings for historical climate change (Deser et al., 2020a). In CESM2-SFLE, the GHG (AAER) simulation is forced with time-evolving GHG (AAER) forcing, with other forcing held fixed at 1850 levels (i.e., the *forcing-only* experimental setup). We also include the 10-member all-but-aerosols (xAAER; the *all-but-forcing* experimental setup) simulations and follow Deser et al. (2020a) to calculate the contribution of anthropogenic aerosols as the difference between ALL and xAAER (ALL-minus-xAAER). With xAAER and ALL-minus-xAAER, we can assess the robustness of D&A results given the potential non-additivity issue reported in Simpson et al. (2023).

We use the annual SMB, and monthly P, R, TAS, and Z500 from these simulations. Monthly CESM2 outputs are converted to an annual sum (P, R) or annual mean (TAS, Z500) to compare against annual SMB. The area-weighted SMB, P, R (unit: mm per year) is summed over Greenland and divided by the global ocean area derived from the CESM2 land mask to convert into a GMSL equivalent (unit: mm GMSL equivalent per year). This GMSL equivalent is multiplied by 361.8 to convert to Gt per year. Anomalies are calculated by removing the 1958-2019 climatological means for regression analyses.

2.2 Detection and attribution (D&A) approach

D&A is commonly performed with a regression of the observation (y) onto the fingerprint(s) of the external forcing (x_i) as

$$y = \sum_{i=1}^{m} \beta_i x_i + \epsilon_y \quad (1)$$

where β_i is the scaling factor(s) to best match the time-dependent fingerprint(s) to the observation, the fingerprint(s) x_i are usually estimated by averaging many simulations (e.g., ensemble mean), and ϵ_y is the residual not explained by the simulated forced response (e.g., internal variability)(Allen and Scott, 2003; Swart et al., 2018). In this paper, we treat the RACMO-ERA simulation as y as there is no in-situ observation of GrIS SMB at the temporal and spatial coverages necessary for this D&A analysis; x_i are estimated by ensemble mean of CESM2-LE and CESM2-SFLE. For the univariate case ($i = 1$), x_i is estimated by the ensemble mean from ALL as x_{ALL}; for the bivariate case ($i = 2$), x_i are estimated by the ensemble mean from GHG and AAER as x_{GHG} and x_{AAER} (or x_{xAAER} and $x_{ALL-minus-xAAER}$). Eq. (1) can be solved by performing an ordinary least squares (OLS) regression with y and x_i. In this case, we assume x_i is observed without uncertainty. When β_i is significantly larger than 0, the forced response from fingerprint(s) x_i is considered detectable; when β_i is not significantly different from 1, the forced response is considered attributable to the fingerprint(s) x_i. The significance level of β_i is usually determined from the distribution of β_i due to internal variability, estimated from climate models (e.g., from pre-industrial simulations (*PiControl*) or historical simulations from which the ensemble mean has been removed), and follows the IPCC guidance to indicate the significance of β_i and the confidence of attributing this signal to a given forcing(s).

In practice, x_i contains uncertainties, such as from the choice of climate models and the errors due to averaging over a finite number of ensemble members. A total least square (TLS) regression is a common solution to perform D&A to account for uncertainty in x_i (Allen and Scott 2003; Kirchmeier-Young et al., 2017; Schurer et al., 2013). Eq. (1) can be rewritten as

$$y = \sum_{i=1}^{m} \beta_i (x_i - \epsilon_{x_i}) + \epsilon_y \tag{2}$$

where now, ϵ_{x_i} is introduced to account for the uncertainties in simulated forced response in x_i. A singular value decomposition (SVD) on the system of equations can solve β_i in a deterministic way for the TLS regression (Allen and Scott, 2003).

The choice of whether to use an OLS or TLS regression should be made with caution, as TLS regression is not necessarily preferred over OLS for climate change D&A (McKitrick 2023). For example, the deterministic solutions of TLS regression can be considered as a linear transformation of OLS regression coefficients and, mathematically, such a transformation could introduce an upward bias for the regression coefficients, leading to a potential false positive in D&A when determining β_i with TLS regression (McKitrick 2023). Moreover, climate models have biases in simulating the internal variability, either too large or too small a magnitude, which makes estimating the significance level of β_i from internal variability based on that from climate models an imperfect approach.

In this study, we instead construct a Bayesian TLS regression to reduce bias and account for the uncertainty from using a climate model large ensemble from a single model (CESM2-LE and CESM2-SFLE). We first construct an ensemble of numerical experiments for an ideal case of one-dimensional linear regression $y = \beta x$ where both sampled data y and x have noise (see Supplementary Information). This experiment confirms that the deterministic TLS regression solution overestimates the regression coefficients when compared with OLS regression and that our Bayesian TLS regression can alleviate this upward bias (Figure S1). We also calculate the scaling factor for attributing GrIS SMB changes to ALL historical forcings with CESM2-LE with a deterministic OLS regression, a deterministic TLS regression, and a Bayesian TLS regression (Figure S2). Our results demonstrate that our Bayesian TLS regression provides the most conservative estimate of the significance level of β_i and does not overestimate the scaling factor in the same way as the deterministic TLS solution (Figure S2).

2.2.1 Bayesian TLS regression

A Bayesian TLS regression with a Markov Chain Monte Carlo (MCMC) technique is used to address concerns of using a deterministic TLS regression for D&A (Katzfuss et al., 2017). With prior knowledge about the data and the uncertainty it might introduce for the D&A analysis, we define three parameters to set up the Bayesian TLS regression: the scaling factors (β_i), the uncertainty of estimating the true forced response with CESM2-LE and CESM2-SFLE (σ_x), and the uncertainty of observing the true forced response in the reference data (i.e., usually due to internal variability; σ_y). With a Bayesian TLS regression, the parameters in a regression model (β_i, σ_x, σ_y) are estimated in a probabilistic way, with the priors of their distributions determined from the data from RACMO-ERA, CESM2-LE, and CESM2-SFLE. In addition, a latent variable, $x_{latent} \sim \mathcal{N}(x, \sigma_x^2)$, is introduced to represent an unknown true forced response(s) from CESM2-LE/CESM2-SFLE (i.e., x_{latent}, the true unknown fingerprint(s), is a draw from a normal distribution with mean determined by x with a spread of σ_x). Therefore, we formulate the D&A with

$$x_{latent} \sim \mathcal{N}(x_{ensmean}, (\frac{\sigma_{x_{ensmean}}}{\sqrt{n}})^2) \tag{3}$$

The mean of x_{latent} is estimated by the ensemble mean from the simulation(s) used for D&A ($x_{ensmean}$) with a spread defined as the standard error of the estimated forced response from that ensemble mean ($\frac{\sigma_{x_{ensmean}}}{\sqrt{n}}$), where n is the number of ensemble members. With the assumption of the posterior distribution of y as

$$y \sim \mathcal{N}(\beta x_{latent}, \sigma_y^2) \tag{4}$$

the Bayesian TLS regression coefficient (β_i) is solved with PyMC. Technical details (including the setup for priors) and idealized numerical experiments can be found in the Supplementary Information.

In this paper, we use the Bayesian TLS regression to obtain 10,000 posterior samples of β_i so that we can estimate the confidence level of the attribution based on the posterior distributions of β_i. This Bayesian TLS regression is also applied to estimate the temperature sensitivity of SMB and R to TAS in the reference data and the forced responses simulated by CESM2 (see Table S1 for setups of priors).

3 Results

3.1 Decadal variability in GMSL due to GrIS SMB changes

Reconstruction data from Frederikse et al., (2020) shows that total GrIS mass loss has decadal variability and this decadal variability comes from the anomalous SMB relative to its long-term climatology (Figure 1; correlation coefficient between SMB and total mass loss is 0.72, *p < 0.01*, at interannual time scales; 0.92, *p < 0.01*, for 10-year running means with effective degree of freedom, eDOF, reduced to 6). For example, there are positive SMB anomalies during 1970-2000, slowing the rise in

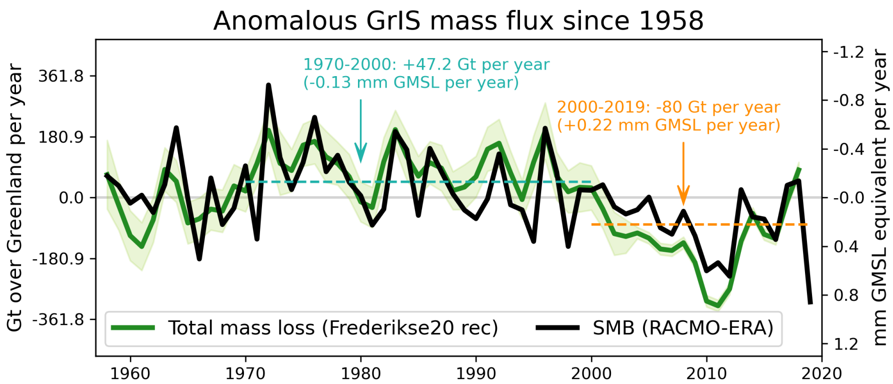

Figure 1. Decadal variability in GrIS' contribution to Global Mean Sea Level (GMSL) is observable and explained by decadal variability in surface mass balance (SMB). The anomalous (long-term mean subtracted) annual GrIS mass loss from the Frederikse et al., (2020) reconstruction (green) and the anomalous annual GrIS SMB simulated by RACMO with ERA5 reanalysis (RACMO-ERA; black). The thick green lines are the 5000-member ensemble mean values of Frederikse et al. (2020) reconstruction, and the shadings are ± 1 standard deviation across the 5000 ensemble members.

GMSL due to GrIS mass loss (Figure 1); in turn, the greater decline in SMB after 2000 leads to an accelerated rise in GMSL contributed by the GrIS. We note that the high correlations between the total mass loss from Frederikse et al. (2020) and the RACMO-simulated SMB reported here could also be influenced by the fact that reconstructed GrIS mass loss data includes RACMO-simulated SMB.

3.2 Detection and attribution of historical GrIS SMB changes

CESM2-LE with historical forcing (ALL) simulates a decline in SMB that is most apparent after 1990 (Figure 2a), despite a wide range of internal variability (purple shading) that also covers the interannual variability in RACMO-ERA. According to the D&A framework, the SMB change in RACMO-ERA is detectable and attributable to historical forcing with 99% confidence (i.e., *virtually certain*; Figure 2b). SMB changes can be approximated as precipitation (P) minus runoff (R; Figure S3, temporal correlation coefficient 0.99, $p < 0.01$, and 1.00, $p < 0.01$, for 10-year running mean time series with 6 eDOF), as sublimation contributes <10% of SMB budget (van Kampenhout et al., 2020). The individual time series show that both ALL-forced precipitation and runoff increases (Figure 2c, 2e; note that R is inverted). However, this ALL-forced increase in precipitation is not detected in the observation (Figure 2d), meaning the observed variability of precipitation could just be internal variability (see also van Kampenhout et al., 2020). On the other hand, the increase in R is detectable and attributable to ALL historical forcing (Figure 2f; 99% confidence, *virtually certain*), agreeing with previous studies that historical GrIS SMB loss is mainly due to warming-driven runoff changes (Noël et al., 2020; Noël et al., 2019; van Kampenhout et al., 2020).

The GrIS SMB changes from ALL (Figure 2a purple solid line) can be approximated as the sum of the changes from GHG and AAER (Figure S3; temporal correlation coefficient 0.66, $p < 0.01$, for SMB time series from ALL vs GHG+AAER

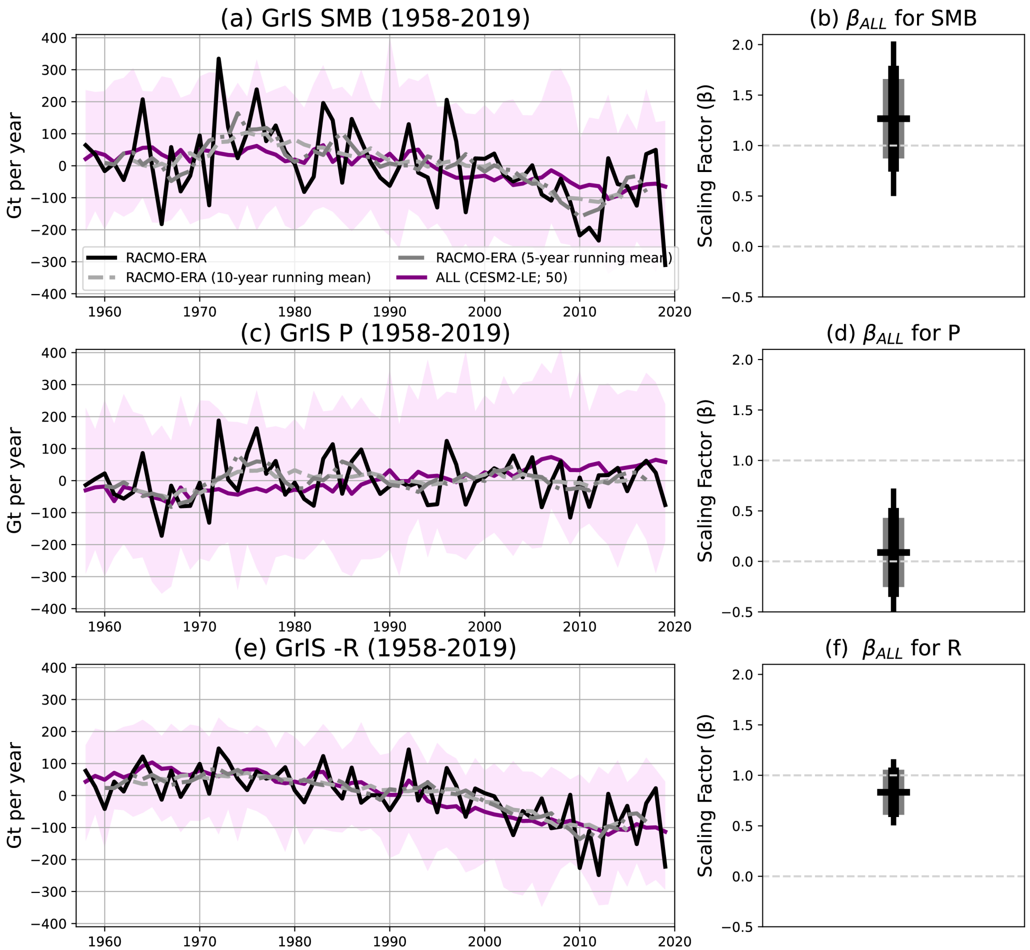

Figure 2. (a, c, e) Time series of GrIS SMB, P, -R since 1958 from RACMO-ERA (black; light gray and gray dashed lines are 10-year and 5-year running mean) and ensemble mean of CESM2-LE (purple). The purple shadings are the full range across ensemble members (i.e., maxima to minima). (b, d, f) Univariate scaling factors (β_{ALL}) of GrIS SMB, P, R. The horizontal line is the mean of the 10,000 posterior samples of β_{ALL}, and the gray shading/thick black vertical line/thin black vertical line is ± 1/ ± 1.64/ ± 2.57 standard deviation of the 10,000 posterior samples of β_{ALL}, indicating the 66%/90%/99% confidence intervals in D&A (*likely*/*very likely*/*virtually certain* based on IPCC guideline). Here, scaling factor (β_{ALL}) is derived by the Bayesian Total Least Square regression with y from RACMO-ERA and x from ensemble mean of CESM2-LE.

and 0.93, $p < 0.01$, for 10-year running means with 6 eDOF), with GHG driving a long-term decline in SMB and AAER contributing to an increase before mid-1980 and a slight decrease thereafter (Figure 3a). Before mid-1980, GHG and AAER basically cancel each other out, while they combine to drive the decline of ALL-forced SMB afterward (Fig. 3a).

A bivariate Bayesian TLS regression is formulated to assess the D&A for these two historical radiative forcings, showing that both GHG (99% confidence, *virtually certain*) and AAER (90% confidence, *very likely*) contribute to the GrIS SMB changes (Figure 3b). Interestingly, the posterior distribution of β_{GHG} has a narrower spread than the posterior distribution of β_{AAER}, implying a lower S/N in detecting the AAER-forced signal in RACMO-ERA SMB changes. Consistent with Figure 2, there is no detectable precipitation change due to neither GHG nor AAER in RACMO-ERA (Figure 3c, 3d). However, there is a detectable GrIS runoff change attributed to both GHG and AAER, but both their influences are potentially underestimated (i.e., β_{GHG} and β_{AAER} are both significantly larger than 1), and β_{AAER} also has a wider spread in its posterior distribution than β_{GHG} for runoff (Figure 3e, 3f).

Studies have shown that CESM2 has nonlinear forced responses due to different climate mean states (Simpson et al., 2023) or the non-additive responses to different forcings (Kuo et al., 2025). Therefore, we repeat the bivariate D&A with SMB, precipitation, and runoff from the xAAER and ALL-minus-xAAER simulations to check the robustness of attributing both anthropogenic aerosols and greenhouse gases when using a climate model (CESM2) with reported nonlinear forced responses. Using xAAER and ALL-minus-xAAER to represent GHG and AAER forcing, this analysis yields robust conclusions: GHG and AAER create forced signals in the historical 1958-2019 GrIS SMB through runoff changes, and the attribution to both xAAER and ALL-minus-xAAER is *virtually certain* (99% confidence; Figure S4). Interestingly, the posterior distribution of $\beta_{ALL-minus-xAAER}$ has a narrower spread for both SMB and runoff compared with the posterior distribution of β_{AAER} (Figure S4b and Figure 3b for SMB and Figure S4f and Figure 3f for runoff), though $\beta_{ALL-minus-xAAER}$ and β_{AAER} still have a wider spread than β_{xAAER} and β_{GHG}. Additionally, runoff changes are not underestimated in ALL-minus-xAAER and xAAER (Figure S4f) as they are in GHG and AAER (Figure 3f), as the means of the posterior bivariate scaling factors are now closer to (1,1). Thus, there appears to be a state dependence of the attribution to AAER.

Overall, our D&A results indicate that historical GrIS SMB changes are attributable to both GHG and AAER through runoff changes. Despite differences in the scaling factors, these attribution results are robust to the sets of single forcing simulations used (*all-but-forcing* or *forcing-only* experimental setups with CESM2). We also point out there is a lower S/N when attributing GrIS SMB changes and runoff changes to AAER compared with attributing to GHG. This lower S/N when attributing to AAER appears in two ways: (1) underestimated response (usually $\beta_{AAER} > 1$ and also $> \beta_{GHG}$) and (2) wider confidence intervals of β_{AAER} than that of β_{GHG}.

3.3 Mean state temperature affects uncertainty in D&A for AAER

GrIS SMB has a stronger sensitivity to warming than to cooling (Thompson-Munson et al., 2024), and runoff has a nonlinear relationship to temperature change (Trusel et al., 2018). This nonlinear runoff response to temperature is commonly seen in cryospheric variables in response to different mean state temperatures (Gottlieb and Mankin 2024) with different energy barrier to overcome and/or different positive degree days to start melting and inducing runoff changes (Sherman et al., 2020). Here, we

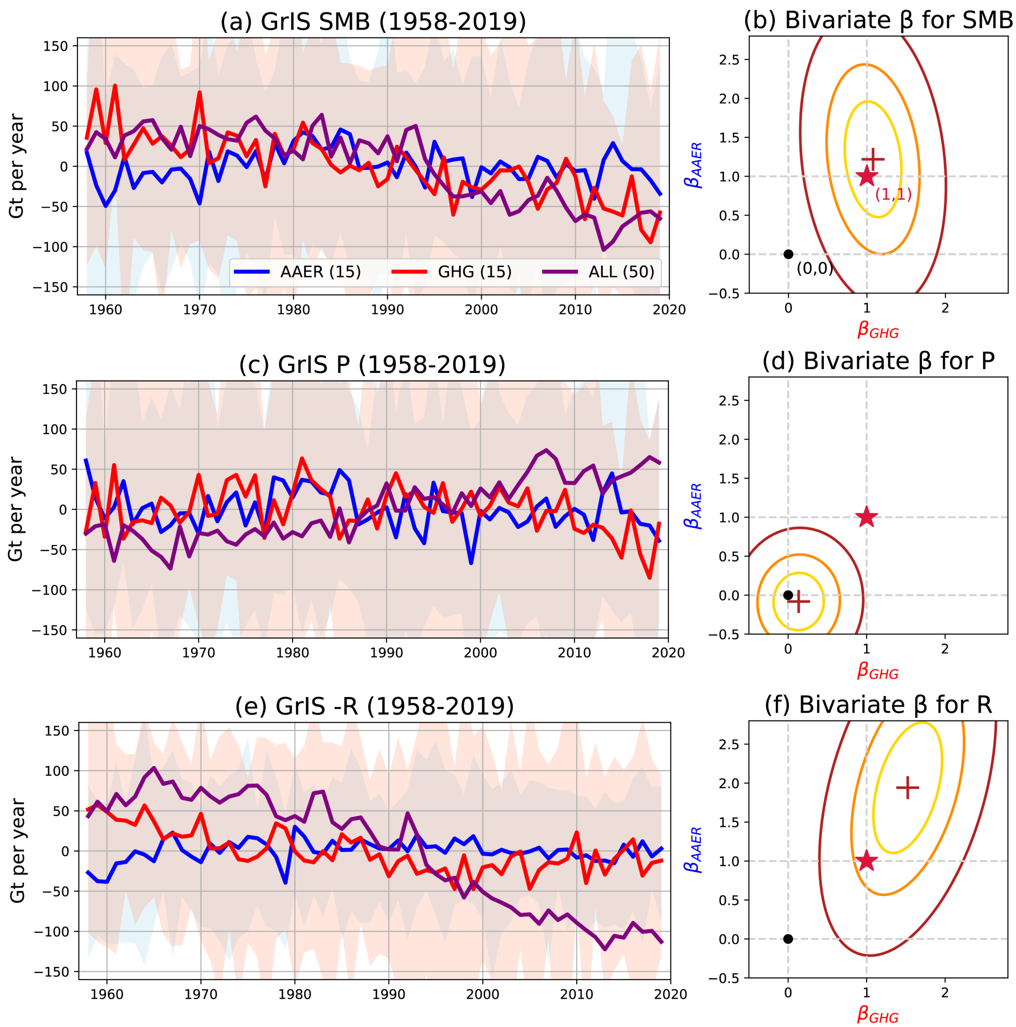

Figure 3. (a, c, e) Time series of GrIS SMB, P, -R since 1958 from ensemble mean of CESM2-SFLE greenhouse gases-only simulation (GHG; red), ensemble mean of CESM2-SFLE anthropogenic aerosols-only simulation (AAER; blue), ensemble mean of CESM2-LE ALL simulation (purple as Figure 2). The red/blue shadings are the full range across ensemble members (i.e., maxima to minima) in GHG/AAER. (b, d, f) Bivariate scaling factors (β_{GHG} and β_{AAER}) of GrIS SMB, P, R. The firebrick plus symbol is the mean of the 10,000 posterior samples of β_{GHG} and β_{AAER}, and the golden/orange/firebrick confidence ellipses are the 66%/90%/99% confidence intervals in β_{GHG} and β_{AAER} for D&A (likely/very likely/virtually certain based on IPCC guideline). When the confidence ellipse includes the point (1,1) (shown as the crimson star) and excludes the origin (0,0) (shown as the black dot), a bivariate attribution to both forcings is established. Here, scaling factors (β_{GHG} and β_{AAER}) are derived by the Bayesian Total Least Square regression with y from RACMO-ERA and x from ensemble mean of AAER and GHG from CESM2-SFLE.

hypothesize that the different temperature sensitivities of runoff in these different simulations might contribute to the lower S/N of the attribution to AAER compared with the attribution to GHG. SMB has a negative temperature sensitivity in RACMO-ERA, ALL, and GHG simulations (Figure 4a), and all of these simulations demonstrate apparent increases in runoff with warming (Figure 4b). However, this negative temperature sensitivity is not seen in the AAER simulation (Figure 4a). There is a nonlinear temperature sensitivity of runoff if the simulations are sorted by their 1958-2019 climatological temperatures (Figure 4b), explaining the lack of negative temperature sensitivity of SMB in AAER (Figure 4a). In addition, the mean temperature over GrIS has a weaker forced response in AAER than in GHG (Figure S5; also true using ALL-minus-xAAER and xAAER). Together with the weaker temperature sensitivity of SMB in AAER due to the weaker temperature sensitivity of runoff, these two factors lead to a generally lower S/N in attributing SMB changes to AAER than GHG. Precipitation sensitivity to warming is generally positive across simulations (Figure S6), as precipitation usually increases under warming (Held and Soden, 2006). Note that precipitation sensitivity is much higher in the ALL-minus-xAAER simulation than in the AAER simulation (Figure S6), explaining the slightly more positive SMB sensitivity in ALL-minus-xAAER (Figure 4a).

This mean state temperature dependent SMB and runoff sensitivity can also explain why the uncertainty ellipse of β using xAAER and ALL-minus-xAAER (Figure S4) is smaller than the uncertainty ellipse using AAER and GHG (Figure 3). This is because xAAER and ALL-minus-xAAER simulations both have higher mean state temperatures than GHG and AAER simulations (orange vs red bars and light blue vs blue bars in Figure 4). The runoff responses are thus stronger in both the xAAER and ALL-minus-xAAER simulations, and therefore easier to detect; β_{xAAER} and $\beta_{ALL-minus-xAAER}$ are both closer to (1,1) with narrower posterior distributions (Figure 3f vs Figure S4f). Although the attribution to AAER is robust across *all-but-forcing* or *forcing-only* experimental setups in CESM2, these results demonstrate that mean state temperatures in different simulations can affect their runoff responses and therefore our confidence in attributing SMB changes to that forcing with this D&A framework.

3.4 Atmospheric drivers of forced GrIS runoff changes

What are the mechanisms by which GHG and AAER forcing drive long-term trends and decadal variability in GrIS SMB through runoff changes? Here, we focus on the summer (JJA) temperature and circulation patterns, which are linked to the melting-induced runoff changes (Sherman et al., 2020; Hanna et al., 2014; Tedesco and Fettweis 2020). The trend map for 1958-2019 from ERA5 shows overall JJA polar warming and increasing Z500 over Greenland (Figure 5a), consistent with the Greenland Block Index (GBI) time series (Figure S7a). The correlation between annual GrIS runoff and JJA near-surface temperature and JJA Z500 from ERA5 is positive, i.e., a Greenland blocking pattern (Figure 5e). Greenland blocking provides more cloudless days and subsidence-induced warming (Sherman et al., 2020), as well as warm air advection towards Western Greenland (Hanna et al., 2014; Tedesco and Fettweis 2020) due to the anti-cyclone over Greenland. The correlation pattern in ERA5 remains consistent even after detrending and temporal smoothing (Figure S8). Thus, the long-term linear trend has little impact on the correlation pattern seen in ERA5.

JJA near-surface warming and Z500 increasing trends over the North Atlantic sector are visible in both ALL (Figure 5b) and GHG (Figure 5c). Though the ALL-forced Z500 trend is weaker than the observed Z500 trend (consistent with GBI in

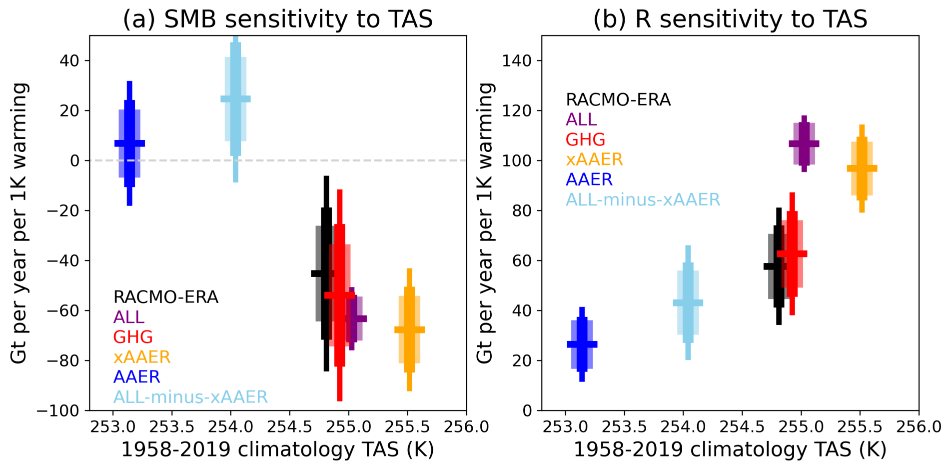

Figure 4. (a) The observed (RACMO-ERA; black) and forced (ALL, GHG, xAAER, AAER, ALL-minus-xAAER; purple, red, orange, blue, light blue respectively) GrIS SMB sensitivity to near-surface temperature during 1958-2019 sorted by the climatological mean near-surface temperature. (b) The observed (RACMO-ERA; black) and forced GrIS R sensitivity to near-surface temperature during 1958-2019 sorted by the climatological mean near-surface temperature. Here, SMB and R sensitivities are derived by the Bayesian Total Least Square regression with SMB or R as y and TAS as x from RACMO, the ensemble mean of CESM2-LE, or the ensemble mean of CESM2-SFLE as appropriate.

Figure S7 and Delhasse et al. (2020)), the observed trend is within the range of possible trends from the 50-member ALL ensemble. The forced temperature and Z500 trends from ALL and GHG are overall alike, confirming that GHG contributes to the long-term linear trend seen in these atmospheric variables related to GrIS runoff changes.

In addition, the Subpolar Gyre cooling correlates with a more positive NAO (Fan et al., 2023). This implies a less negative NAO/reduced Greenland blocking as a result of this air-sea coupled feedback over the Subpolar Gyre, which may explain why GHG-forced runoff (Figure 3e) and GBI (Figure S7b) plateaus after 2000 when the Subpolar Gyre cooling intensifies. This is also supported by the significant correlations of an emerging Greenland blocking pattern in GHG that differs from its uniform warming and Z500 trends (Figure 5c), regardless of whether linear trends in GHG are removed or not (Figure S9). Although beyond the scope of this study, idealized experiments to distinguish the circulation changes originating from direct GHG radiative forcing versus from GHG-induced Subpolar Gyre SSTs would help advance understanding of Greenland circulation and GrIS mass loss.

AAER, on the other hand, contributes almost nothing to this long-term trend pattern (Figure 5a vs 5d). These trend maps imply that the detected signal from AAER during 1958-2019 (Figure 3b, 3f) does not arise through the long-term linear trend but through forced decadal variability undergoing phase changes during this time period. We compare maps of the correlation from ERA5 (Figure 5e) and from the ensemble mean of AAER during 1958-2019 (Figure 5f). The AAER-based correlation map shows a pattern that is distinct from its long-term trend (Figure 5f vs Figure 5d); instead, the correlation map shows a pattern more similar to the ERA5-based correlation map (Figure 5e vs 5f). Both ERA5 and AAER have positive correlations

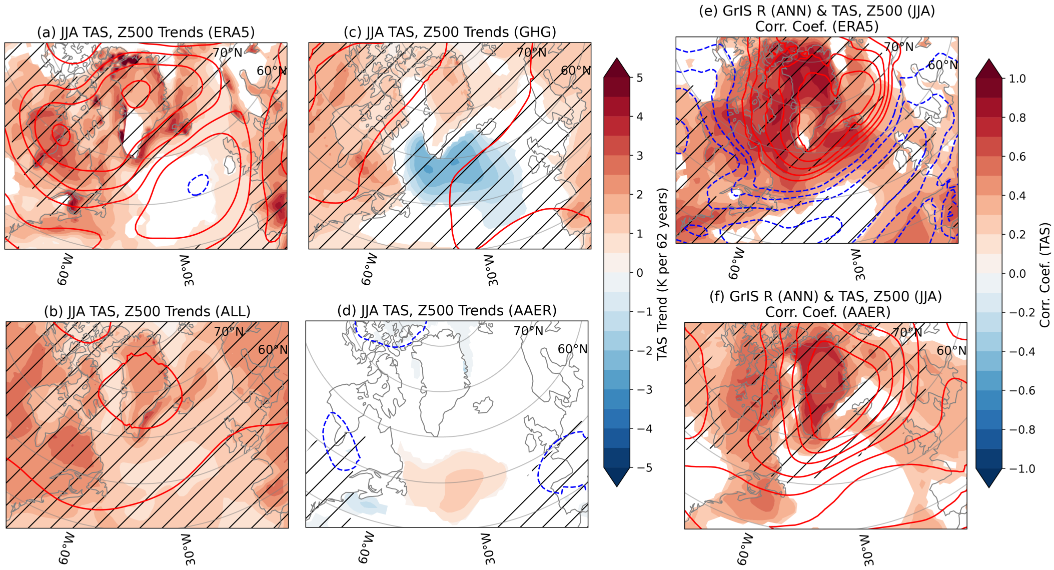

Figure 5. Trend maps of 500 hPa geopotential height (Z500; contours) and near-surface air temperature (TAS; shading) during 1958-2019 in (a) ERA5 reanalysis, (b) ensemble mean of all forcings CESM2-LE simulation (50; ALL), (c) ensemble mean of GHG-only simulation (15; GHG), and (d) ensemble mean of AAER-only simulation (15; AAER). Grid cells with insignificant TAS trends are masked out (95% confidence for ERA5, and ensemble mean trend over 1 standard deviation across all trends in the ensemble for climate model simulations). Grid cells with significant Z500 trends are hatched (95% confidence for ERA5 and ensemble mean trend over 1 standard deviation across all possible trends in the ensemble for climate model simulations). Z500 contours start from ± 10 (m per 62 years) with contour spacing of 10 (m per 62 years). (e-f) Correlation map of GrIS R with Z500 (contours) and TAS (shading) during 1958-2019 in (e) ERA5 reanalysis and (f) 15-member mean AAER. Insignificant TAS correlations are masked out and significant Z500 correlations are hatched (95% confidence). Contours start from 0.1 with contour spacing of 0.1. The significance level of the correlation coefficients is based on a *t-test* with the degrees of freedom corresponding to the length of data (1958-2019, 62 years).

between GrIS runoff and near-surface temperature and Z500. Figure 5f confirms a similar correlation pattern due to AAER, supporting an AAER-forced change in the variability of circulation, imprinted onto a pattern that reinforces Greenland blocking consistent with (Maddison et al., 2024).

4 Discussion and Conclusion

In this paper, we formulate a D&A analysis with CESM2-LE and CESM2-SFLE to investigate 1958-2019 GrIS SMB change and show that the historical SMB change is attributable not only to GHG but also to AAER. To our knowledge, this is the first manuscript demonstrating that parts of the historical GrIS SMB change are attributable to AAER. Specifically, GHG drives the long-term SMB decline, while AAER contributes to the decadal variability of SMB, consistent with a growing literature on how AAER induces decadal variations to other aspects of historical North Atlantic climate change (Scaife and Smith et al., 2018).

To understand the mechanisms of forced SMB change, we consider two perspectives. First, from a mass balance perspective, we demonstrate that the historical forced SMB changes in a ERA5 reanalysis-based RACMO simulation are mainly driven by runoff changes, irrespective of the underlying forcing (GHG or AAER). Second, we investigate the atmospheric pathways by which these forcings affect runoff, demonstrating that the GHG-forced runoff change is mainly driven by long-term warming and the AAER-driven runoff change relates to atmospheric circulation variability of Greenland blocking on decadal time scales (Sherman et al., 2020; Brils et al., 2023; Hanna et al., 2022). These results highlight that different climate forcings can drive SMB changes through different physical mechanisms, with different spatial patterns and time scales (i.e., long-term trend vs decadal variability).

Attribution of regional climate change to AAER often has a low S/N compared to GHG attribution (e.g., Marvel et al., 2019) and our study confirms this tendency. In the case of attributing GrIS SMB, this is due to the temperature sensitivity of runoff being weaker in AAER than GHG, as the sensitivity strongly depends on mean state temperatures in each simulation. We compare the sets of *forcing-only* (GHG and AAER) and *all-but-forcing* (xAAER and ALL-minus-xAAER) CESM2 experiments, where we show robust attribution of historical GrIS SMB changes to both GHG and AAER through runoff changes. The mean state temperature dependency of runoff response can also explain the difference of S/N in the *forcing-only* and *all-but-forcing* sets, as their mean state temperatures are different. Although we show that both AAER and GHG contribute to the historical GrIS SMB changes, such a mean state temperature dependence of the forced SMB response implies a potential bias in the current D&A framework - certain forcings, such as GHG, can individually create a mean state with a stronger response that is more likely to be attributed. Future work will need to develop D&A methods that can systematically account for mean state temperature dependency in climate responses.

CESM2 and RACMO simulate reasonable SMB and water budgets (Noël et al., 2018; an Kampenhout et al., 2020); however, both are subject to model structural uncertainty. The model structural uncertainty accounts for most of the uncertainty in SMB future projections (Holube et al., 2022). The high model structural uncertainty in SMB does not come from the snow parameterization uncertainty (Holube et al., 2022). Instead, it comes from atmospheric variables, as GrIS precipitation, temperature, and Z500 all show high model structural uncertainties in their future projections (Zhang et al., 2024). One motivation to conduct D&A with Bayesian regression, instead of a deterministic regression, is to account for the uncertainty in estimates of forced responses (from CESM2) and of observations (from RACMO). We acknowledge the caveat that this study does not fully sample model structural uncertainty. Future work to extend D&A with more climate models could enhance the robustness of the results presented here. Such efforts could also support the development of observational constraints on SMB projections, for example, based on the temperature sensitivity presented here.

On top of the different runoff responses due to the mean state temperature dependence, we note that historical aerosol emissions used in CMIP6 simulations have large uncertainties, especially pre-1980 (Mahowald et al., 2024). Beyond the scope of this paper, future works should thus explore the impacts of aerosol emissions and forcing uncertainties on D&A of GrIS SMB changes.

The mean state temperature dependency of runoff found in our study implies that GrIS SMB changes might accelerate in the future, especially as we expect continued increases in greenhouse gases with simultaneous reductions in anthropogenic aerosols (Samset et al., 2018; Persad et al., 2022). Thus, under stronger warming in these future projections, further growth in the contribution of GrIS SMB reduction to GMSL rise is foreseeable.

Data availability. The global mean sea level (GMSL) contributed by Greenland Ice Sheet (GrIS) reconstruction dated back to 1900 is taken from Frederikse et al. (2020) with their data publicly accessible from Zenodo (https://zenodo.org/records/3862995). RACMO-ERA from https://zenodo.org/records/7100706. Instruction on how to access data from Community Earth System Model version 2 large ensemble and single forcing large ensemble can be found https://www.cesm.ucar.edu/community-projects/lens2/data-sets.

Author contributions. All the authors were involved in the conceptualization of this project, the discussion of the interpretations of results, and the revision of the drafts. YNK analyzed the data, created the visualization, and wrote the first draft of the manuscript.

Acknowledgements. Riley Culberg was supported in part by NASA grants 80NSSC24K1445 and 80NSSC24K1037. The authors appreciate insightful discussions with Lorenzo Polvani, You-Ting Wu, Angeline Pendergrass, John Fasullo, William Lipscomb, and Natalie Mahowald when preparing the manuscript. The authors also thank the editor and reviewers for their constructive feedback during the revision to improve the manuscript.

5 Reference

Allen, M. R. and Stott, P. A.: Estimating signal amplitudes in optimal fingerprinting, part I: theory, Climate Dynamics, 21, 477–491, https://doi.org/10.1007/s00382-003-0313-9, 2003.

Bamber, J. L., Westaway, R. M., Marzeion, B., and Wouters, B.: The land ice contribution to sea level during the satellite era, Environ. Res. Lett., 13, 063008, https://doi.org/10.1088/1748-9326/aac2f0, 2018.

Brils, M., Kuipers Munneke, P., and Van Den Broeke, M. R.: Spatial Response of Greenland's Firn Layer to NAO Variability, JGR Earth Surface, 128, e2023JF007082, https://doi.org/10.1029/2023JF007082, 2023.

Chen, X., Zhang, X., Church, J. A., Watson, C. S., King, M. A., Monselesan, D., Legresy, B., and Harig, C.: The increasing rate of global mean sea-level rise during 1993–2014, Nature Clim Change, 7, 492–495, https://doi.org/10.1038/nclimate3325, 2017.

Church, J. A., White, N. J., Konikow, L. F., Domingues, C. M., Cogley, J. G., Rignot, E., Gregory, J. M., Van Den Broeke, M. R., Monaghan, A. J., and Velicogna, I.: Revisiting the Earth's sea-level and energy budgets from 1961 to 2008: SEA-LEVEL AND ENERGY BUDGETS, Geophys. Res. Lett., 38, n/a-n/a, https://doi.org/10.1029/2011GL048794, 2011.

Danabasoglu, G., Lamarque, J. -F., Bacmeister, J., Bailey, D. A., DuVivier, A. K., Edwards, J., Emmons, L. K., Fasullo, J., Garcia, R., Gettelman, A., Hannay, C., Holland, M. M., Large, W. G., Lauritzen, P. H., Lawrence, D. M., Lenaerts, J. T. M., Lindsay, K., Lipscomb, W. H., Mills, M. J., Neale, R., Oleson, K. W., Otto-Bliesner, B., Phillips, A. S., Sacks, W., Tilmes, S., Kampenhout, L., Vertenstein, M., Bertini, A., Dennis, J., Deser, C., Fischer, C., Fox-Kemper, B., Kay, J. E., Kinnison, D., Kushner, P. J., Larson, V. E., Long, M. C., Mickelson, S., Moore, J. K., Nienhouse, E., Polvani, L., Rasch, P. J., and Strand, W. G.: The Community Earth System Model Version 2 (CESM2), J. Adv. Model. Earth Syst., 12, https://doi.org/10.1029/2019MS001916, 2020.

Dangendorf, S., Hendricks, N., Sun, Q., Klinck, J., Ezer, T., Frederikse, T., Calafat, F. M., Wahl, T., and Törnqvist, T. E.: Acceleration of U.S. Southeast and Gulf coast sea-level rise amplified by internal climate variability, Nat Commun, 14, 1935, https://doi.org/10.1038/s41467-023-37649-9, 2023.

Delhasse, A., Hanna, E., Kittel, C., and Fettweis, X.: Brief communication: CMIP6 does not suggest any atmospheric blocking increase in summer over Greenland by 2100, Intl Journal of Climatology, 41, 2589–2596, https://doi.org/10.1002/joc.6977, 2021.

Deser, C., Lehner, F., Rodgers, K. B., Ault, T., Delworth, T. L., DiNezio, P. N., Fiore, A., Frankignoul, C., Fyfe, J. C., Horton, D. E., Kay, J. E., Knutti, R., Lovenduski, N. S., Marotzke, J., McKinnon, K. A., Minobe, S., Randerson, J., Screen, J. A., Simpson, I. R., and Ting, M.: Insights from Earth system model initial-condition large ensembles and future prospects, Nat. Clim. Chang., 10, 277–286, https://doi.org/10.1038/s41558-020-0731-2, 2020a.

Deser, C., Phillips, A. S., Simpson, I. R., Rosenbloom, N., Coleman, D., Lehner, F., Pendergrass, A. G., DiNezio, P., and Stevenson, S.: Isolating the Evolving Contributions of Anthropogenic Aerosols and Greenhouse Gases: A New CESM1 Large Ensemble Community Resource, Journal of Climate, 33, 7835–7858, https://doi.org/10.1175/JCLI-D-20-0123.1, 2020b.

Dittus, A. J., Hawkins, E., Robson, J. I., Smith, D. M., and Wilcox, L. J.: Drivers of Recent North Pacific Decadal Variability: The Role of Aerosol Forcing, Earth's Future, 9, https://doi.org/10.1029/2021EF002249, 2021.

Dong, B. and Sutton, R. T.: Recent trends in summer atmospheric circulation in the North Atlantic/European region: is there a role for anthropogenic aerosols?, Journal of Climate, 1–49, https://doi.org/10.1175/JCLI-D-20-0665.1, 2021.

Dow, W. J., Maycock, A. C., Lofverstrom, M., and Smith, C. J.: The Effect of Anthropogenic Aerosols on the Aleutian Low, Journal of Climate, 34, 1725–1741, https://doi.org/10.1175/JCLI-D-20-0423.1, 2021.

Enderlin, E. M., Howat, I. M., Jeong, S., Noh, M., Van Angelen, J. H., and Van Den Broeke, M. R.: An improved mass budget for the Greenland ice sheet, Geophysical Research Letters, 41, 866–872, https://doi.org/10.1002/2013GL059010, 2014.

Fan, Y., Liu, W., Zhang, P., Chen, R., and Li, L.: North Atlantic Oscillation contributes to the subpolar North Atlantic cooling in the past century, Clim Dyn, 61, 5199–5215, https://doi.org/10.1007/s00382-023-06847-y, 2023.

Frederikse, T., Landerer, F., Caron, L., Adhikari, S., Parkes, D., Humphrey, V. W., Dangendorf, S., Hogarth, P., Zanna, L., Cheng, L., and Wu, Y.-H.: The causes of sea-level rise since 1900, Nature, 584, 393–397, https://doi.org/10.1038/s41586-020-2591-3, 2020.

Gottlieb, A. R. and Mankin, J. S.: Evidence of human influence on Northern Hemisphere snow loss, Nature, 625, 293–300, https://doi.org/10.1038/s41586-023-06794-y, 2024.

Hanna, E., Fettweis, X., Mernild, S. H., Cappelen, J., Ribergaard, M. H., Shuman, C. A., Steffen, K., Wood, L., and Mote, T. L.: Atmospheric and oceanic climate forcing of the exceptional Greenland ice sheet surface melt in summer 2012, Intl Journal of Climatology, 34, 1022–1037, https://doi.org/10.1002/joc.3743, 2014.

Hanna, E., Cropper, T. E., Hall, R. J., Cornes, R. C., and Barriendos, M.: Extended North Atlantic Oscillation and Greenland Blocking Indices 1800–2020 from New Meteorological Reanalysis, Atmosphere, 13, 436, https://doi.org/10.3390/atmos13030436, 2022.

Hay, C. C., Morrow, E., Kopp, R. E., and Mitrovica, J. X.: Probabilistic reanalysis of twentieth-century sea-level rise, Nature, 517, 481–484, https://doi.org/10.1038/nature14093, 2015.

He, C., Clement, A. C., Kramer, S. M., Cane, M. A., Klavans, J. M., Fenske, T. M., and Murphy, L. N.: Tropical Atlantic multidecadal variability is dominated by external forcing, Nature, 622, 521–527, https://doi.org/10.1038/s41586-023-06489-4, 2023.

Held, I. M. and Soden, B. J.: Robust Responses of the Hydrological Cycle to Global Warming, Journal of Climate, 19, 5686–5699, https://doi.org/10.1175/JCLI3990.1, 2006.

Hersbach, H., Bell, B., Berrisford, P., Hirahara, S., Horányi, A., Muñoz-Sabater, J., Nicolas, J., Peubey, C., Radu, R., Schepers, D., Simmons, A., Soci, C., Abdalla, S., Abellan, X., Balsamo, G., Bechtold, P., Biavati, G., Bidlot, J., Bonavita, M., Chiara, G., Dahlgren, P., Dee, D., Diamantakis, M., Dragani, R., Flemming, J., Forbes, R., Fuentes, M., Geer, A., Haimberger, L., Healy, S., Hogan, R. J., Hólm, E., Janisková, M., Keeley, S., Laloyaux, P., Lopez, P., Lupu, C., Radnoti, G., Rosnay, P., Rozum, I., Vamborg, F., Villaume, S., and Thépaut, J.: The ERA5 global reanalysis, Q.J.R. Meteorol. Soc., 146, 1999–2049, https://doi.org/10.1002/qj.3803, 2020.

Hofer, S., Lang, C., Amory, C., Kittel, C., Delhasse, A., Tedstone, A., and Fettweis, X.: Greater Greenland Ice Sheet contribution to global sea level rise in CMIP6, Nat Commun, 11, 6289, https://doi.org/10.1038/s41467-020-20011-8, 2020.

Hwang, Y.-T., Xie, S.-P., Chen, P.-J., Tseng, H.-Y., and Deser, C.: Contribution of anthropogenic aerosols to persistent La Niña-like conditions in the early 21st century, Proc. Natl. Acad. Sci. U.S.A., 121, e2315124121, https://doi.org/10.1073/pnas.2315124121, 2024.

IPCC, 2023: Climate Change 2023: Synthesis Report. Contribution of Working Groups I, II and III to the Sixth Assessment Report of the Intergovernmental Panel on Climate Change [Core Writing Team, H. Lee and J. Romero (eds.)]. IPCC, Geneva, Switzerland, pp. 35-115, doi: 10.59327/IPCC/AR6-9789291691647.

Kang, J. M., Shaw, T. A., and Sun, L.: Anthropogenic Aerosols Have Significantly Weakened the Regional Summertime Circulation in the Northern Hemisphere During the Satellite Era, AGU Advances, 5, e2024AV001318, https://doi.org/10.1029/2024AV001318, 2024.

Katzfuss, M., Hammerling, D., and Smith, R. L.: A Bayesian hierarchical model for climate change detection and attribution, Geophysical Research Letters, 44, 5720–5728, https://doi.org/10.1002/2017GL073688, 2017.

Kirchmeier-Young, M. C., Zwiers, F. W., and Gillett, N. P.: Attribution of Extreme Events in Arctic Sea Ice Extent, Journal of Climate, 30, 553–571, https://doi.org/10.1175/JCLI-D-16-0412.1, 2017. Kjeldsen, K. K., Korsgaard, N. J., Bjørk, A. A., Khan, S. A., Box, J. E., Funder, S., Larsen, N. K., Bamber, J. L., Colgan, W., Van Den Broeke, M., Siggaard-Andersen, M.-L., Nuth, C., Schomacker, A., Andresen, C. S., Willerslev, E., and Kjær, K. H.: Spatial and temporal distribution of mass loss from the Greenland Ice Sheet since AD 1900, Nature, 528, 396–400, https://doi.org/10.1038/nature16183, 2015.

Kuo, Y., Kim, H., and Lehner, F.: Anthropogenic Aerosols Contribute to the Recent Decline in Precipitation Over the U.S. Southwest, Geophysical Research Letters, 50, e2023GL105389, https://doi.org/10.1029/2023GL105389, 2023.

Kuo, Y.-N., Lehner, F., Simpson, I. R., Deser, C., Phillips, A. S., Newman, M., Shin, S.-I., Wong, S., and Arblaster, J. M.: Recent southwestern US drought exacerbated by anthropogenic aerosols and tropical ocean warming, Nat. Geosci., 18, 578–585, https://doi.org/10.1038/s41561-025-01728-x, 2025.

Liang, Y.-C., Frankignoul, C., Kwon, Y.-O., Gastineau, G., Manzini, E., Danabasoglu, G., Suo, L., Yeager, S., Gao, Y., Attema, J. J., Cherchi, A., Ghosh, R., Matei, D., Mecking, J. V., Tian, T., and Zhang, Y.: Impacts of Arctic Sea Ice on Cold Season Atmospheric Variability and Trends Estimated from Observations and a Multi-model Large Ensemble, Journal of Climate, 1–64, https://doi.org/10.1175/jcli-d-20-0578.1, 2021.

Lipscomb, W. H., Price, S. F., Hoffman, M. J., Leguy, G. R., Bennett, A. R., Bradley, S. L., Evans, K. J., Fyke, J. G., Kennedy, J. H., Perego, M., Ranken, D. M., Sacks, W. J., Salinger, A. G., Vargo, L. J., and Worley, P. H.: Description and evaluation of the Community Ice Sheet Model (CISM) v2.1, Geosci. Model Dev., 12, 387–424, https://doi.org/10.5194/gmd-12-387-2019, 2019.

Luu, L. N., Hanna, E., De Alwis Pitts, D., Maddison, J., Screen, J. A., Catto, J. L., and Fettweis, X.: Greenland summer blocking characteristics: an evaluation of a high-resolution multi-model ensemble, Clim Dyn, 62, 10503–10523, https://doi.org/10.1007/s00382-024-07453-2, 2024.

Maddison, J. W., Catto, J. L., Hanna, E., Luu, L. N., and Screen, J. A.: Missing Increase in Summer Greenland Blocking in Climate Models, Geophysical Research Letters, 51, e2024GL108505, https://doi.org/10.1029/2024GL108505, 2024.

Mahowald, N. M., Li, L., Albani, S., Hamilton, D. S., and Kok, J. F.: Opinion: The importance of historical and paleoclimate aerosol radiative effects, Atmos. Chem. Phys., 24, 533–551, https://doi.org/10.5194/acp-24-533-2024, 2024.

Marvel, K., Cook, B. I., Bonfils, C. J. W., Durack, P. J., Smerdon, J. E., and Williams, A. P.: Twentieth-century hydroclimate changes consistent with human influence, Nature, 569, 59–65, https://doi.org/10.1038/s41586-019-1149-8, 2019.

McKenna, C. M. and Maycock, A. C.: Sources of Uncertainty in Multimodel Large Ensemble Projections of the Winter North Atlantic Oscillation, Geophysical Research Letters, 48, e2021GL093258, https://doi.org/10.1029/2021GL093258, 2021.

McKitrick, R.: On the choice of TLS versus OLS in climate signal detection regression, Clim Dyn, 60, 359–374, https://doi.org/10.1007/s 022-06315-z, 2023.

Mitrovica, J. X., Tamisiea, M. E., Davis, J. L., and Milne, G. A.: Recent mass balance of polar ice sheets inferred from patterns of global sea-level change, Nature, 409, 1026–1029, https://doi.org/10.1038/35059054, 2001.

Mouginot, J., Rignot, E., Bjørk, A. A., Van Den Broeke, M., Millan, R., Morlighem, M., Noël, B., Scheuchl, B., and Wood, M.: Forty-six years of Greenland Ice Sheet mass balance from 1972 to 2018, Proc. Natl. Acad. Sci. U.S.A., 116, 9239–9244, https://doi.org/10.1073/pnas.1904242116, 2019.

Noël, B., Van De Berg, W. J., Van Wessem, J. M., Van Meijgaard, E., Van As, D., Lenaerts, J. T. M., Lhermitte, S., Kuipers Munneke, P., Smeets, C. J. P. P., Van Ulft, L. H., Van De Wal, R. S. W., and Van Den Broeke, M. R.: Modelling the climate and surface mass balance of polar ice sheets using RACMO2 – Part 1: Greenland (1958–2016), The Cryosphere, 12, 811–831, https://doi.org/10.5194/tc-12-811-2018, 2018. Noël, B., Van De Berg, W. J., Lhermitte, S., and Van Den Broeke, M. R.: Rapid ablation zone expansion amplifies north Greenland mass loss, Sci. Adv., 5, eaaw0123, https://doi.org/10.1126/sciadv.aaw0123, 2019.

Noël, B., Van Kampenhout, L., Van De Berg, W. J., Lenaerts, J. T. M., Wouters, B., and Van Den Broeke, M. R.: Brief communication: CESM2 climate forcing (1950–2014) yields realistic Greenland ice sheet surface mass balance, The Cryosphere, 14, 1425–1435, https://doi.org/10.5194/tc-14-1425-2020, 2020.

Noël, B., Lenaerts, J. T. M., Lipscomb, W. H., Thayer-Calder, K., and Van Den Broeke, M. R.: Peak refreezing in the Greenland firn layer under future warming scenarios, Nat Commun, 13, 6870, https://doi.org/10.1038/s41467-022-34524-x, 2022.

Oudar, T., Kushner, P. J., Fyfe, J. C., and Sigmond, M.: No Impact of Anthropogenic Aerosols on Early 21st Century Global Temperature Trends in a Large Initial-Condition Ensemble, Geophys. Res. Lett., 45, 9245–9252, https://doi.org/10.1029/2018GL078841, 2018.

Pattyn, F., Ritz, C., Hanna, E., Asay-Davis, X., DeConto, R., Durand, G., Favier, L., Fettweis, X., Goelzer, H., Golledge, N. R., Kuipers Munneke, P., Lenaerts, J. T. M., Nowicki, S., Payne, A. J., Robinson, A., Seroussi, H., Trusel, L. D., and Van Den Broeke, M.: The Greenland and Antarctic ice sheets under 1.5 °C global warming, Nature Clim Change, 8, 1053–1061, https://doi.org/10.1038/s41558-018-0305-8, 2018.

Persad, G. G., Samset, B. H., and Wilcox, L. J.: Aerosols must be part of climate risk assessments, 2022.

Rodgers, K. B., Lee, S.-S., Rosenbloom, N., Timmermann, A., Danabasoglu, G., Deser, C., Edwards, J., Kim, J.-E., Simpson, I. R., Stein, K., Stuecker, M. F., Yamaguchi, R., Bódai, T., Chung, E.-S., Huang, L., Kim, W. M., Lamarque, J.-F., Lombardozzi, D. L., Wieder, W. R., and Yeager, S. G.: Ubiquity of human-induced changes in climate variability, Earth Syst. Dynam., 12, 1393–1411, https://doi.org/10.5194/esd-12-1393-2021, 2021.

Samset, B. H., Sand, M., Smith, C. J., Bauer, S. E., Forster, P. M., Fuglestvedt, J. S., Osprey, S., and Schleussner, C. -F.: Climate Impacts From a Removal of Anthropogenic Aerosol Emissions, Geophysical Research Letters, 45, 1020–1029, https://doi.org/10.1002/2017GL076079, 2018.

Scaife, A. A. and Smith, D.: A signal-to-noise paradox in climate science, npj Clim Atmos Sci, 1, 28, https://doi.org/10.1038/s41612-018-0038-4, 2018.

Schurer, A. P., Hegerl, G. C., Mann, M. E., Tett, S. F. B., and Phipps, S. J.: Separating Forced from Chaotic Climate Variability over the Past Millennium, Journal of Climate, 26, 6954–6973, https://doi.org/10.1175/JCLI-D-12-00826.1, 2013.

Sherman, P., Tziperman, E., Deser, C., and McElroy, M.: Historical and Future Roles of Internal Atmospheric Variability in Modulating Summertime Greenland Ice Sheet Melt, Geophysical Research Letters, 47, e2019GL086913, https://doi.org/10.1029/2019GL08 2020.

Simpson, I. R., Rosenbloom, N., Danabasoglu, G., Deser, C., Yeager, S. G., McCluskey, C. S., Yamaguchi, R., Lamarque, J.-F., Tilmes, S., Mills, M. J., and Rodgers, K. B.: The CESM2 Single-Forcing Large Ensemble and Comparison to CESM1: Implications for Experimental Design, Journal of Climate, 36, 5687–5711, https://doi.org/10.1175/JCLI-D-22-0666.1, 2023.

Swart, N. C., Gille, S. T., Fyfe, J. C., and Gillett, N. P.: Recent Southern Ocean warming and freshening driven by greenhouse gas emissions and ozone depletion, Nature Geosci, 11, 836–841, https://doi.org/10.1038/s41561-018-0226-1, 2018.

Takahashi, C. and Watanabe, M.: Pacific trade winds accelerated by aerosol forcing over the past two decades, Nature Clim Change, 6, 768–772, https://doi.org/10.1038/nclimate2996, 2016.

Tedesco, M. and Fettweis, X.: Unprecedented atmospheric conditions (1948–2019) drive the 2019 exceptional melting season over the Greenland ice sheet, The Cryosphere, 14, 1209–1223, https://doi.org/10.5194/tc-14-1209-2020, 2020.

Thompson-Munson, M., Kay, J. E., and Markle, B. R.: Greenland's firn responds more to warming than to cooling, The Cryosphere, 18, 3333–3350, https://doi.org/10.5194/tc-18-3333-2024, 2024.

Trusel, L. D., Das, S. B., Osman, M. B., Evans, M. J., Smith, B. E., Fettweis, X., McConnell, J. R., Noël, B. P. Y., and Van Den Broeke, M. R.: Nonlinear rise in Greenland runoff in response to post-industrial Arctic warming, Nature, 564, 104–108, https://doi.org/10.1038/s41586-018-0752-4, 2018.

van Kampenhout, L., Lenaerts, J. T. M., Lipscomb, W. H., Lhermitte, S., Noël, B., Vizcaíno, M., Sacks, W. J., and van den Broeke, M. R.: Present-Day Greenland Ice Sheet Climate and Surface Mass Balance in CESM2, JGR Earth Surface, 125, e2019JF005318, https://doi.org/10.1029/2019JF005318, 2020.

Wdowinski, S., Bray, R., Kirtman, B. P., and Wu, Z.: Increasing flooding hazard in coastal communities due to rising sea level: Case study of Miami Beach, Florida, Ocean & Coastal Management, 126, 1–8, https://doi.org/10.1016/j.ocecoaman.2016.03.002, 2016.

Wu, Y., Liang, Y., Kuo, Y., Lehner, F., Previdi, M., Polvani, L. M., Lo, M., and Lan, C.: Exploiting SMILEs and the CMIP5 Archive to Understand Arctic Climate Change Seasonality and Uncertainty, Geophysical Research Letters, 50, e2022GL100745, https://doi.org/10.1029/2022GL100745, 2023.